

This discussion paper is/has been under review for the journal Solid Earth (SE).
Please refer to the corresponding final paper in SE if available.

High-precision relocation of seismic sequences above a dipping Moho: the case of the January–February 2014 seismic sequence in Cephalonia Isl. (Greece)

V. K. Karastathis, E. Mouzakiotis, A. Ganas, and G. A. Papadopoulos

National Observatory of Athens, Institute of Geodynamics, Lofos Nymfon, P.O. Box 20048, 11810, Athens, Greece

Received: 5 August 2014 – Accepted: 27 August 2014 – Published: 2 September 2014

Correspondence to: V. K. Karastathis (karastathis@noa.gr)

Published by Copernicus Publications on behalf of the European Geosciences Union.

2699

Abstract

Detailed velocity structure and Moho mapping is of crucial importance for a high precision relocation of seismicity occurring out of, or marginally to, the geometry of seismological networks, such as at the boundary of converging plates. The crustal thinning from the plate boundary towards the back-arc area creates significant errors in accurately locating the earthquake, especially when distant seismic phases are included in the analysis. The case of the Cephalonia (Ionian Sea, Greece) sequence of January–February 2014 provided an excellent example where locations were greatly affected by the crustal thinning from the plate boundary at the Ionian sea towards the Aegean sea. This effect was examined in detail by testing various velocity models of the region in order to determine an optimal model. Our tests resulted in the adoption of a velocity model that resembles the crustal thinning of the region. Then, a relocation procedure was performed in the Cephalonia sequence for the time period from 26 January 2014 to 15 May 2014 by applying probabilistic non-linear location algorithms. The high-precision relocation resulted in an improved spatial distribution of the seismicity with respect to the preliminary locations and provided a reliable basis to examine seismotectonic implications of the Cephalonia sequence.

1 Introduction

On 26 January (13:55:42 and 18:45:08 GMT) and 3 February 2014 (3:08:44 GMT) western Cephalonia Isl., Ionian Sea (Greece), (Fig. 1) was ruptured by three strong earthquakes of magnitudes M_w 6.0, M_w 5.3 and M_w 5.9, respectively (Table 1, Fig. 2). The two strongest earthquakes caused considerable damage in buildings and infrastructure as well as several types of ground failures (rock-falls, landslides, soil liquefaction) in Paliki peninsula, mainly in Lixouri town and the surrounding villages (Papadopoulos et al., 2014; Valkaniotis et al., 2014) (Fig. 1). The Peak Ground Acceleration (PGA) recorded in several localities at accelerometric stations, operated by the

2700

zonally layered Earth. For example, the crustal thickness is strongly affected in areas situated in the vicinity of convergent plate boundaries. This is the case of the thick continental Aegean crust in the vicinity of the Hellenic subduction zone. In fact, the compressional regime along the Hellenic Arc leads to folding and thin-skinned tectonics as well as to the creation of the Mediterranean ridge, which evolved to an accretionary prism, and to subsequent thickening of the crust (Underhill, 1989; Yem et al., 2011). Crustal surveys have shown that in western Greece, where the oceanic crust of the African plate is sliding beneath the Aegean area, the continental crustal thickness exceeds 40 km and becomes progressively thinner to the east (Makris, 1978; Tsokas and Hansen, 1997; Papazachos and Nolet, 1997; Tiberi et al., 2001; Karagianni et al., 2005; Pearce et al., 2012). At the South Aegean Sea region the crustal thickness reaches values as low as 20 km or less (Makris 1975, 1976, 1977; Bohnhoff et al. 2001; Tirel et al., 2004). Thus, when an earthquake occurs in the thick part of the crust and the wave-paths of the first arriving waves pass through the Moho that progressively becomes shallower, the travel-time errors may increase considerably with the increase of the epicentral distance. In contrast, shallower events are not so strongly affected, particularly in short epicentral distances since only *Pg* phases are actually picked. This structure causes an asymmetrical shape to the head-wave wavefront. Due to this structure, the adoption of a 1-D velocity model (see NOA-IG model in Fig. 3) can cause systematic travel time residuals in the events location.

3 Analysis of seismological data

The Cephalonia 2014 seismic sequence was examined exactly in this context. The first strong earthquake of 26 January 2014 was recorded by the permanent stations of the HUSN (Hellenic Unified Seismological Network; <http://www.gein.noa.gr/en/networks/husn/>) before the installation of the portable network in Cephalonia. The focus of that event was preliminary determined by NOAGI at a location situated about 5 km NNE from the city of Argostoli and at focal depth of $h = 21$ km (Fig. 2) (Table 1). This location

2703

falls clearly outside of the aftershock cloud as well as far from the Lixouri town, where the macroseismic epicenter was placed according to the field observations performed by Papadopoulos et al. (2014) (Fig. 2). The epicentral area is situated at the geometrical edge of the permanent network in the sense that no stations were situated to the west of the earthquake focus. Consequently, the azimuthal coverage was poor, leading to unstable location solutions. In addition, the preliminary solution included several phases from significantly large epicentral distances extending up to 360 km, where the crustal thickness was significantly smaller than that in the subduction regime of western Cephalonia. The 1-D model used by NOAGI (Fig. 3), with the Moho boundary placed at 40 km, could not match *Pn* phase data from areas of thin crust, particularly at large epicentral distances. Therefore, significant errors were involved and consequently the epicenter of the first strong earthquake was shifted substantially to the east. Its aftershocks, however, were not shifted significantly because of their small magnitudes that limited epicentral distances over which they were recorded. In a next paragraph it is explained more precisely how errors are introduced in the epicentral solution.

Regarding the preliminary epicenter of the strong (M_w 5.3) aftershock of 26.1.2014 (18:45:08 GMT), it is noticeable that it was located in a better agreement with the macroseismic epicenter (Fig. 2) although it was calculated before the installation of the portable network in Cephalonia. This is explained by the fact that its actual focal depth was shallower than that of the first strong earthquake. It is also worth mentioning that two seconds after the first strong shock of the 26 January 2014, another strong aftershock occurred. Unfortunately, the waveform of this event partially overlapped with the waveform of the first strong shock, making an accurate estimation of its local and moment magnitudes quite difficult. A rough estimation of its duration magnitude gives M_d 5.0. This is consistent with the accounts of local people reporting that a few seconds after the first major event another shock was strongly felt in Cephalonia.

After the installation of the portable network in western Cephalonia the maximum azimuthal gap was decreased significantly, becoming less than 180° for most of the seismic events. The preliminary focus of the strong earthquake (M_w 5.9) of 3 Febru-

2704

ary 2014 was located at shallower depth ($h = 11$ km, Table 1) but within the aftershock cloud (Fig. 2) and at a position close to its macroseismic epicenter which again was placed (Papadopoulos et al., 2014) in Lixouri town.

To effectively relocate the hypocenter data of the sequence one may use a velocity model resembling as much as possible the real velocity structure. An effective model can compensate for most of the systematic time residuals created at distant stations. An alternative method is to use a 1-D model, having found however the epicentral distance range where the effect of the inclined Moho does not considerably affect the location accuracy. This approach limits the seismic phases taken into account. It is reasonably expected that the two different approaches should lead to quite similar results.

4 Selection of velocity model – relocation of the Cephalonia 2014 earthquake sequence

For western Greece, including the area of Cephalonia, only few seismic velocity models have been proposed (Hirn et al., 1996; Haslinger et al., 1999; Sachpazi et al., 2000). The model proposed by Hirn et al. (1996) was directly based on the results of the crustal seismic surveys carried-out during 1992 in the frame of the project STREAMERS. The profile ION-7, with bearing of $N62^\circ E$, was conducted offshore between Cephalonia and Zakynthos (Zante) islands having total length of 180 km, starting from the deep Ionian basin and reaching the western Gulf of Patras (see maps in Hirn et al., 1996). For the data acquisition the Geco-Prakla's M/V *Bin Hai 511* was used with a 36-airgun tuned array (for processing details see also in Kokinou et al., 2005). The 30-fold seismic profile acquired, provided useful information for the shallower structure. However, no precise information was gathered for the Moho interface. To get a rough estimate of the Moho depth, Hirn et al. (1996) performed ray-tracing modeling of the wide-angle traveltimes data, recorded at distant on-shore stations positioned at the Greek mainland. Those stations were located only at the eastern side of the profile. Furthermore assumptions were made for the velocity values beneath the 7 km depth.

2705

Thus, these authors discussed a model with the lower crustal interface (V_p between 5.8 and 6.8 km s^{-1}) at 15 km depth and the Moho boundary at 25 km. Since the structure in this model was almost horizontal, the 1-D model of Fig. 3 can be easily derived.

The velocity model of Haslinger et al. (1999) (Fig. 3) was built for the region at the east of Lefkada Isl., western Greece, which as regards to the Cephalonia 2014 sequence, concentrates a high percentage of the ray-paths between the earthquakes and the stations. This model was built as a “1-D minimum velocity model” for this region by VELEST algorithm (Kissling et al., 1994; Kissling, 1995) and used in a following stage as initial model in the local earthquake tomography method and SIMULPS code (Thurber, 1993; Eberhart-Phillips, 1990, 1993), implemented to calculate the 3-D crustal velocity structure. The SIMULPS code uses a linearized damped least-square inversion to solve the non-linear problem of the hypocentral location and velocity model. Because of this non-linear nature of the problem, the initial velocity model and the initial hypocenter locations in the inversion procedure should be as close as possible to their true values. The “1-D minimum velocity model” calculated by the VELEST algorithm can provide a good approximation and be used as an initial velocity model. The minimum 1-D velocity models are usually used for seismicity relocation (e.g. Lippitsch et al., 2005; Ganas et al., 2014).

The model proposed by Sachpazi et al. (2000) (Fig. 3) was also created by the VELEST algorithm in order to be used as initial model in a 3-D local earthquake tomography performed to determine the velocity structure of the area under study. The procedure for the construction of a 1-D minimum velocity model is highly dependent on the selection of an initial model (Karastathis et al., 2011) and, therefore, it is usually based on the results of seismic profiles. Sachpazi et al. (2000) based their initial model on the seismic profiles presented by Hirn et al. (1996).

For the adoption of an appropriate seismic velocity model we compared the three 1-D models mentioned above (Fig. 3). As we will see later in detail, the model that performed better was the one proposed by Haslinger et al. (1999). With a vertical velocity gradient based on Haslinger et al. (1999) we finally constructed, tested and adopted

2706

a 2-D velocity model with a non-horizontal Moho boundary based on Papazachos and Nolet (1997). Fig. 4 shows the vertical cross-section of the 2-D model.

Before comparing the performance of these models, we examine the influence on the location procedure of the non-horizontal Moho boundary in the Aegean region. More specifically, in order to assess the impact of the errors imposed in the earthquake location procedure by the adoption of a simplified 1-D model, in the presence of a non-horizontal Moho structure, we constructed synthetic arrival times for the adopted model using the 3-D version of the eikonal finite-difference scheme of Podvin and Lecomte (1991) and estimated the time differences for both a horizontal and a non-horizontal Moho structure. The velocity gradient was based on Haslinger et al. (1999). The 2-D model with the non-horizontal Moho boundary is shown in Fig. 4 and the results of the comparison with the respective 1-D are depicted in Fig. 5. As one may expect, the time difference is zero only when the first arrivals are due to the *Pg* seismic phases. Obviously, the shallower events, with focal depth between 5 and 10 km are not affected or affected only slightly, particularly when they do not have enough energy to travel at long epicentral distances. As a result, the majority of the shallow aftershocks remain unaffected. In contrast, the influence is higher for the deeper and stronger events, such as the first strong earthquake of 26 January 2014. For this strong earthquake three different epicenters were calculated with the use of the 1-D model (with the inclusion or the exclusion of distant phases) and with the 2-D model (with all phases) (Fig. 6). It can be seen how the simplified 1-D velocity model affects the epicenter location when distant phases are taken into account. The error decreases when distant phases are omitted.

We concluded that for lack of reliable knowledge regarding the structure and velocity of the Moho boundary and in the presence of poor azimuthal seismographic coverage, it is preferable to limit the range of the epicentral distances of stations used and to base the location mostly on the *Pg* phases.

The data processing has been performed by the NonLinLoc algorithm (Lomax et al., 2000) that follows a non-linear earthquake location method giving a complete prob-

2707

abilistic solution expressed in terms of a posterior density function (PDF) (Tarantola and Valette, 1982). The function is calculated using the Equal Differential Time (EDT) likelihood function and depicted by confidence ellipsoids. Therefore, the higher the confidence of the velocity model, the smaller the ellipsoids of the event locations. This probabilistic approach is characterized by strong advantages as compared with linearized methods. More precisely, the EDT function provides a more reliable uncertainty estimate, especially in the presence of outliers, than the conventional least-squares L1 and L2 norms for the misfit calculation between the observed and calculated travel times. Another advantage of the method is that it is independent on the origin time, so the 4-D problem of hypocenter location reduces to a 3-D search over spatial location of the hypocenter (latitude, longitude, depth). The NonLinLoc algorithm can also use 2-D and 3-D velocity models.

For the relocation of the Cephalonia 2014 aftershock sequence we used NOAGI phase dataset consisting of more than 44 000 *P* wave and 24 000 *S* wave arrivals for the time interval from 26 January 2014 to 15 May 2014 inclusive. Phase data from distant stations ($\Delta > 120$ km) were excluded. It should be noted, however, that small magnitude events remained unaffected since they could hardly be identified at greater epicentral distances anyway.

We compared both the 2-D and 1-D versions of the adopted model with the three models proposed by previous authors (Fig. 3). For the comparison we selected events with at least six *P* and one *S* wave arrivals and azimuthal gap lower than 180° . The station delays were calculated and applied to the location procedure. Station corrections compensate for the effect of the station local geology, which could not be taken into account by the use of 1-D velocity model. The adopted model succeeds in producing a more compact horizontal projection (Fig. 7) and verifies that the aftershock sequence, trending NNE–SSW, covers only the western part of Cephalonia at a length of about 35 km and maximum lateral width of about 10 km. It is noteworthy that the relocated aftershock area nearly coincides with the main part of the macroseismic field that is the area covered by the isoseismal of level V, which is also the area of ground failures pro-

2708

sides, thus leaving an apparent spatial gap between the two clusters. Papadopoulos et al. (2014) suggested that the area of the 2014 gap had already ruptured by the strong (M_w 5.5) strike-slip earthquake of 25 March 2007. However, no temporal relation was found between these two clusters and the occurrence of the strong events of 26 January and 3 February 2014. The north cluster abuts but does not overlap with the southern side of the aftershock area of the 2003 Lefkada Isl. strong (M_w 6.2) mainshock (Papadopoulos et al., 2003) (see also Fig. 13). Besides, the foreshock activity that preceded the first strong earthquake of 26 January 2014 by about four days was recorded exactly in the area of the north (small) aftershock cluster (Papadopoulos et al., 2014). This may indicate that the 2014 activity was initiated at the northern part of the aftershock area where the 2003 Lefkada Isl. activity diminished. Therefore, we observe that a shallow tectonic structure exists in the area of Myrtos Gulf, possibly a near-vertical fault striking WNW-ESE that is perpendicularly to the NNE-SSW strike of the Lefkada 2003 and the Cephalonia 2014 aftershock areas. This fault, which probably controlled the initiation of the 2014 sequence, can be seen in the NNE-SSW cross-section in Fig. 14c that depicts clearly the vertical geometry of the EW cross-fault at Myrtos Gulf, at depths 5–12 km. Evidence also comes from the space-time evolution of the relocated 2014 sequence (Fig. 11) but further examination is needed.

With the relocation applied, the foci of the three strongest earthquakes of the sequence shifted at shallower depths, while the first strong earthquake of 26 January 2014 shifted also towards WNW with respect to the preliminary determinations (Table 1). The thickness of the seismogenic layer does not exceed 16 km. That the 2014 aftershock area was well-formed from the very beginning without spatial expansion after the strong earthquake of 3 February 2014 provides evidence that this earthquake ruptured within the aftershock volume of the 26 January 2014 earthquake which was the largest event of the sequence. From this point of view we may consider that the 3 February event was the strongest aftershock of the sequence that ruptured at shallower depth and at different fault from that of the mainshock of 26 January 2014.

2711

To further control the fault patterns associated with the 26 January and 3 February earthquakes we constructed two respective vertical cross sections as shown in Fig. 14. One may observe that in the section corresponding to the mainshock of 26 January, the aftershocks up to 30 January included in a ± 4 km wide zone seem rather arranged in a plane of nearly N–S direction and dip of about 65° to the east (Fig. 14a). The preferred fault-plane adopted by Papadopoulos et al. (2014) and Valkaniotis et al. (2014) is of strike 23° and dip 68° to the east, which is consistent with the geometry represented by the vertical section. However, the vertical section through the hypocentre of the 3 February 2014 event (Fig. 14b) shows that the fault plane strikes nearly N–S but its dip is about 65° to the west. The geometry of this fault plane is compatible with the fault plane that dips 56° to the west according to the focal mechanism computed by the GFZ ($183^\circ / 56^\circ / 138^\circ$; reported at the European – Mediterranean Seismological Centre (EMSC) website <http://www.emsc-csem.org/Earthquake/mtfull.php?id=357329>). The western dip in combination with the oblique-slip rake may result in uplift of the hangingwall (western) part of the N–S fault during co-seismic motion.

Our relocation procedure suggests a different fault model than that of Karakostas et al. (2014; their Fig. 8) who suggested a right-step of CTFZ, onshore Paliki peninsula. On the contrary, we image the activation of two, blind strike-slip faults along the N-S axis at Myrtos Gulf – Lixouri line, possibly overlapping with a left step. The 26 January 2014 activated fault (Fig. 14a) is in agreement with the blind fault model of Valkaniotis et al. (2014). Such a fault configuration may explain the co-seismic uplift seen on Paliki Peninsula in InSAR data (Boncori et al., manuscript submitted to SRL) as our relocation data in the epicentral region of the 3 February 2014 event point to a west-dipping fault (Fig. 14b). If this is the case, then the hanging wall of this fault moved upwards during co-seismic motion as it is known that Cephalonia region is in state of compression with max. horizontal stress oriented at N78E ($+/- 9$ degrees; Ganas et al., 2013), as determined from GPS data. In addition, Lagios et al. (2012) obtained a N-S discontinuity in their horizontal velocity field (see Fig. 4c of Lagios et al., 2012) across the Gulf

2712

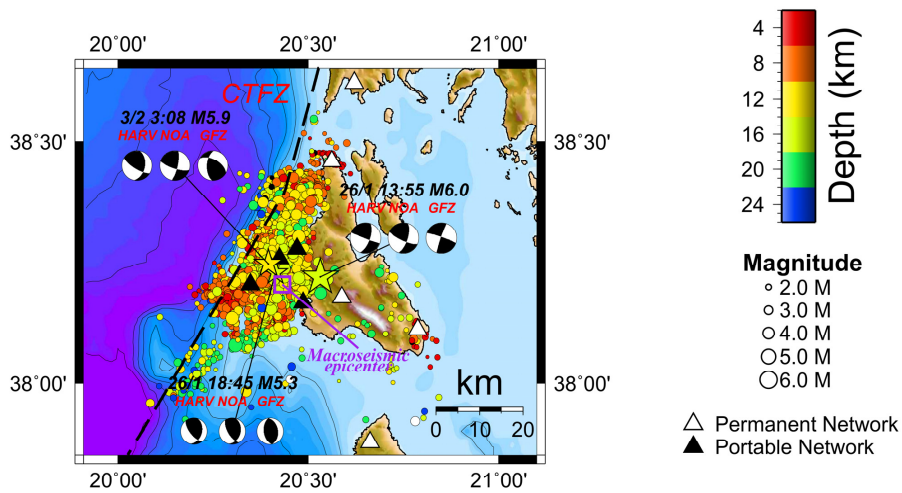


Figure 2. Map of the aftershock sequence from 26 January 2014–15 May 2014 as determined by the National Observatory of Athens. The moment tensor solutions for the largest events as calculated by Global CMT – Harvard University, USA (HARV), National Observatory of Athens (NOA) and GFZ German Research Centre for Geoscience (GeoForschungsZentrums in German) (GFZ).

2721

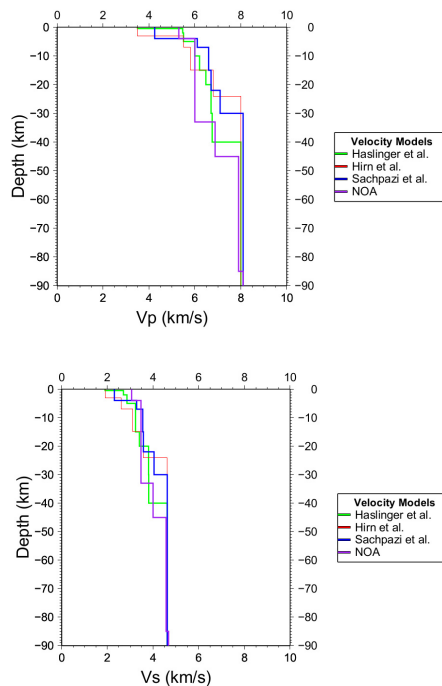


Figure 3. The seismic *P* and *S* wave velocity models tested for the relocation of the aftershock sequence. Green, blue and red correspond to velocity models proposed by Haslinger et al. (1999), Sachpazi et al. (2000), and Hirn et al. (1996), respectively. The model routinely used by NOAGI is marked in purple.

2722

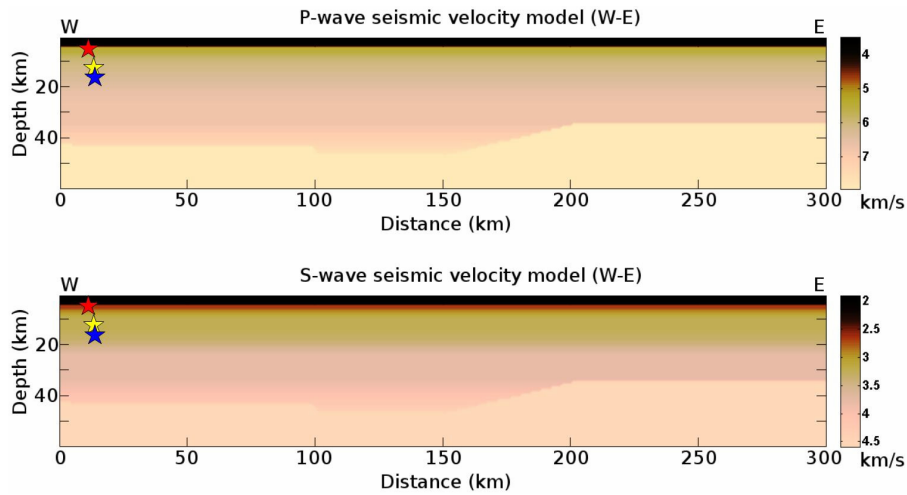


Figure 4. The 2-D velocity model tested to assess the influence of Moho structure. The Moho boundary has been based on the results of Papazachos and Nolet (1997). The position of Cephalonia is between 0–50 km. The hypocenters of the major events are shown with stars (blue for the event of 26 January 2014 (M_w 6.0); yellow for the aftershock of 26 January 2014 (M_w 5.3); red for the event of 3 February 2014 (M_w 5.9).

2723

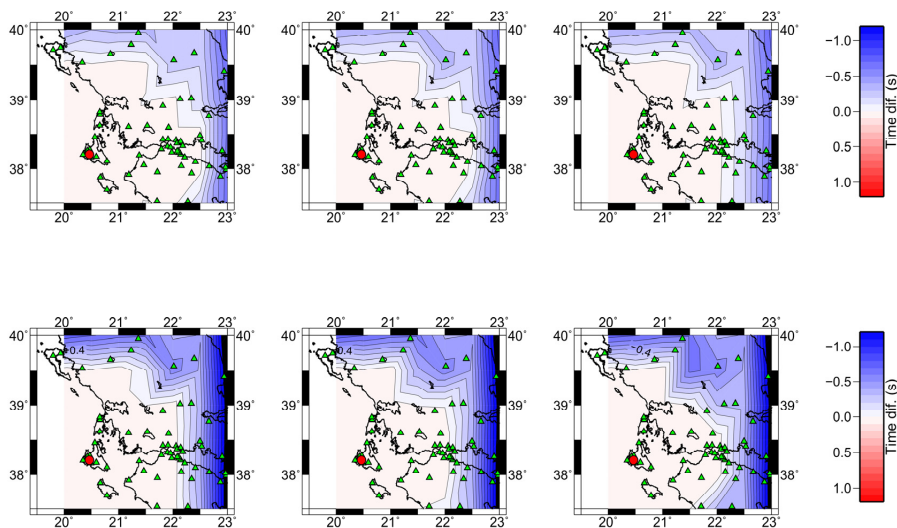


Figure 5. Time differences of P wave (upper panel) and S -wave (lower panel) arrivals between synthetic data calculated on the basis of the 1-D model adopted and the 2-D model based on the same 1-D model but with a non-horizontal Moho boundary. Earthquake focal depths of 5 km (left), 10 km (central) and 15 km (right) are represented. The hypothetical epicentre is shown as red circle. The errors imported in the case which does not take into account the Moho structure can be significant at long distances.

2724

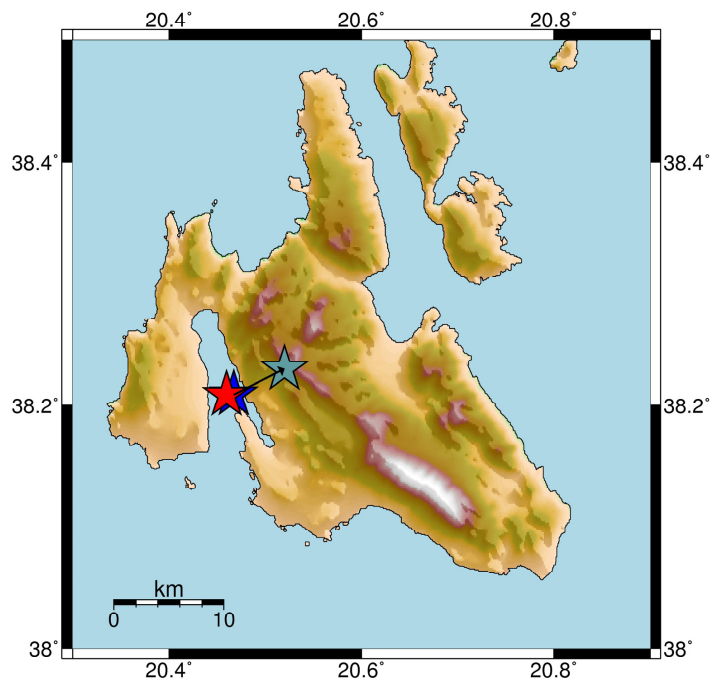


Figure 6. The epicenter of the strong earthquake (M_w 6.0) of 26 January 2014 calculated with the 1-D model of Haslinger et al. (1999) (see Fig. 3) including distant phases (light blue star at the east), the same 1-D model excluding distant phases (blue star at the west), and the 2-D model (see Fig. 4) including distant phases (red star).

2725

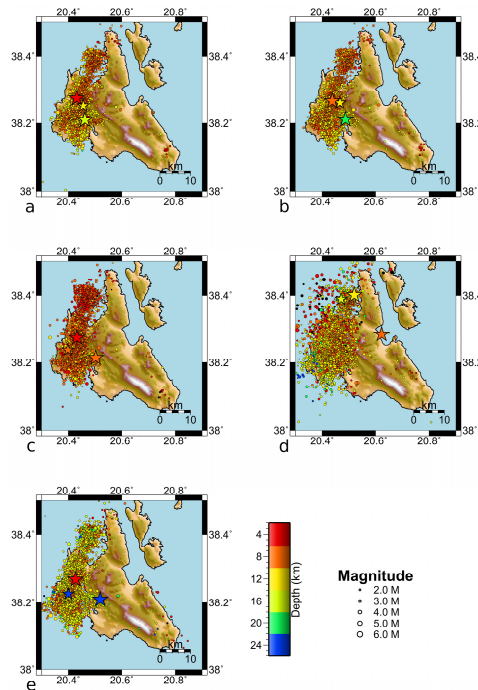


Figure 7. Relocation results by using the velocity models of (a) the 2-D velocity model that resembles the moho structure, (b) the 1-D velocity model proposed by Haslinger et al. (1999), (c) the 1-D velocity model proposed by Sachpazi et al. (2000), (d) the 1-D velocity model proposed by Hirn et al. (1996), (e) the 1-D velocity model used by NOAGI for the daily seismic monitoring.

2726

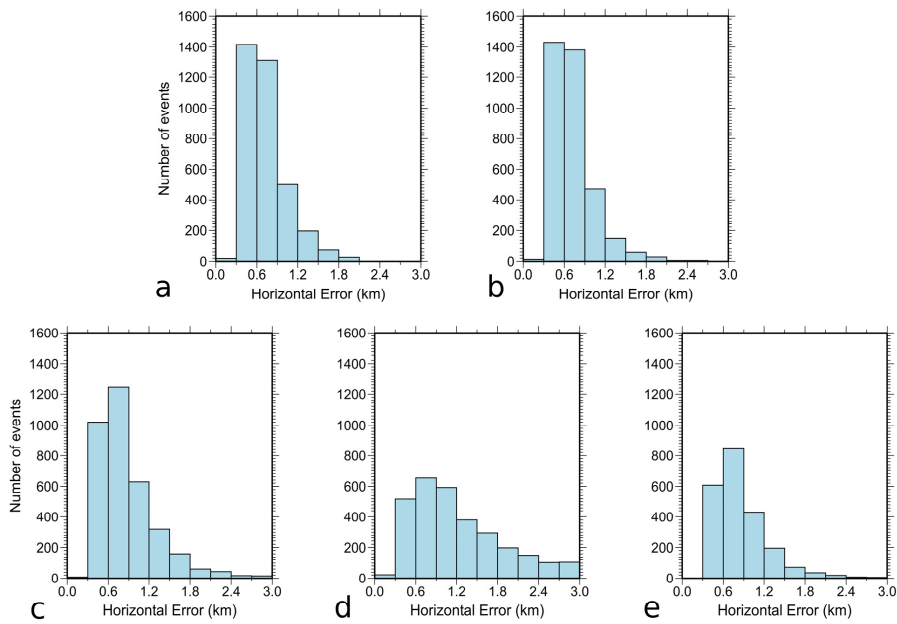


Figure 8. Distribution of the epicenter horizontal error of the relocated Cephalonia 2014 earthquake sequence up to 15.5.2014 for different seismic velocity models: **(a)** adopted 2-D model which is a modification – of the Haslinger et al. (1999) model; **(b)** Haslinger et al. (1999); **(c)** Sachpazi et al. (2000); **(d)** Hirn et al. (1996); **(e)** model routinely used in the daily seismic monitoring by NOAGI.

2727

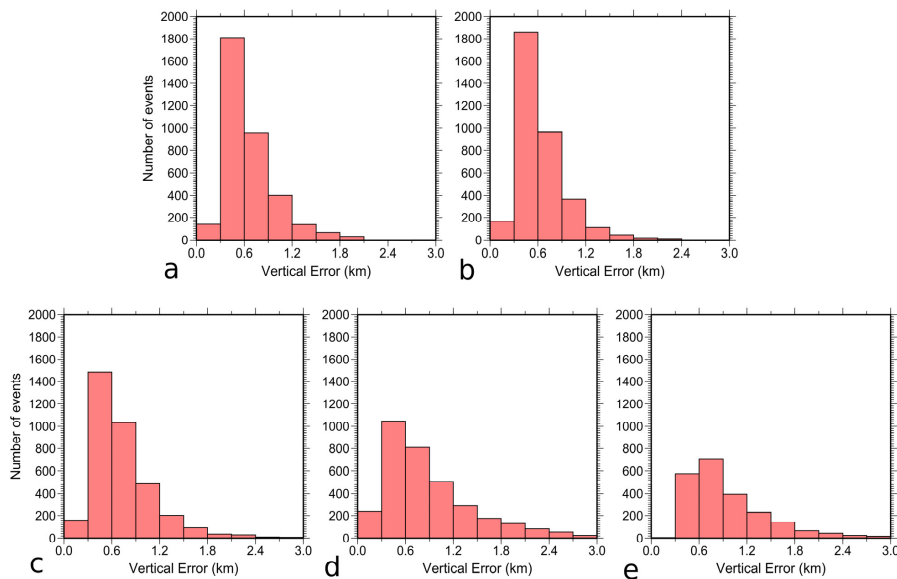


Figure 9. As Fig. 8 for the vertical epicenter error.

2728

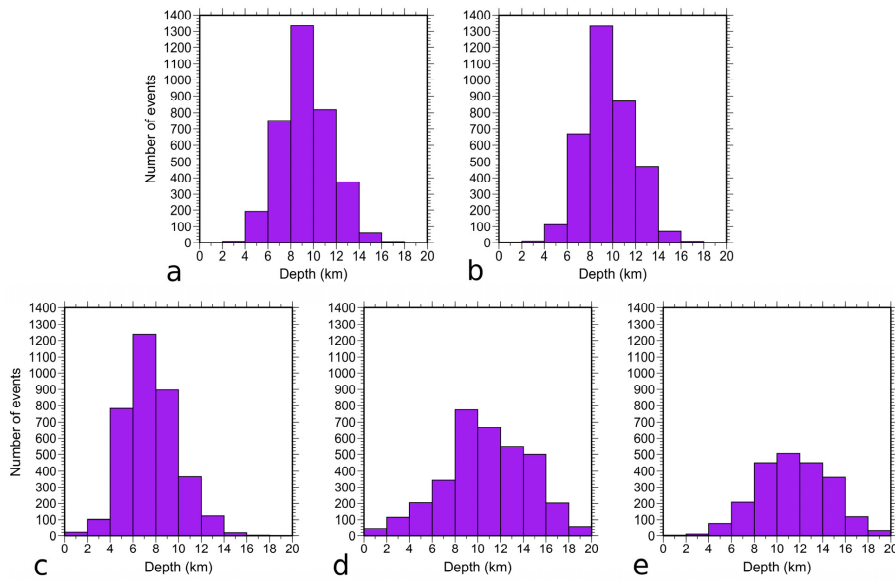


Figure 10. Distribution of hypocentral depth of the relocated Cephalonia 2014 earthquake sequence up to 15 May 2014 for different seismic velocity models: **(a)** adopted 2-D model which is a modification – of the Haslinger et al. (1999) model; **(b)** Haslinger et al. (1999); **(c)** Sachpazi et al. (2000); **(d)** Hirn et al. (1996); **(e)** Model routinely used in the daily seismic monitoring by NOAGI.

2729

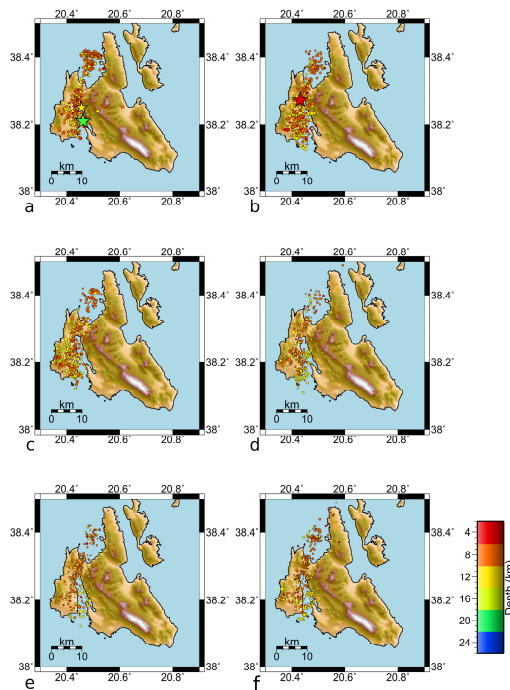


Figure 11. Space-time evolution of the Cephalonia 2014 sequence. The maps show the aftershocks with one week time interval (from **a** to **f**) beginning from 26 January 2014 to 26 March 2014.

2730

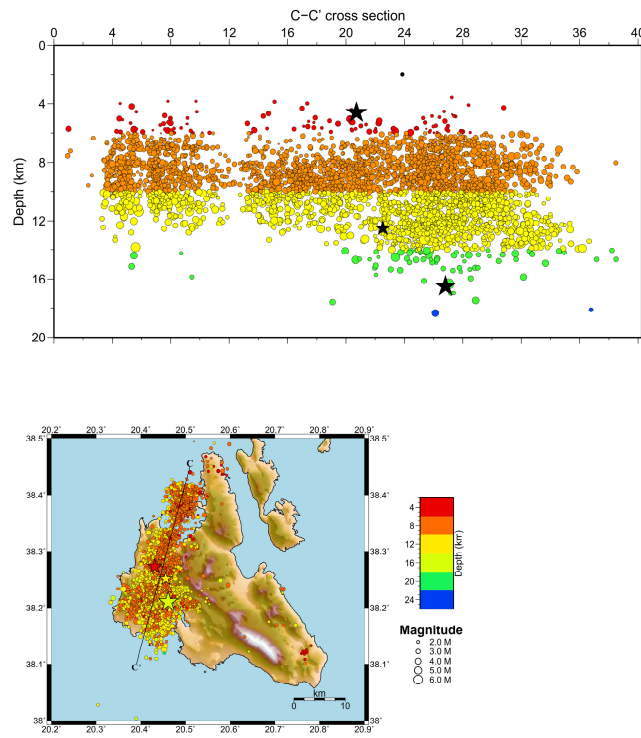


Figure 12. Vertical section of the aftershock sequence during 26 January 2014 to 15 May 2014 and its location map.

2731

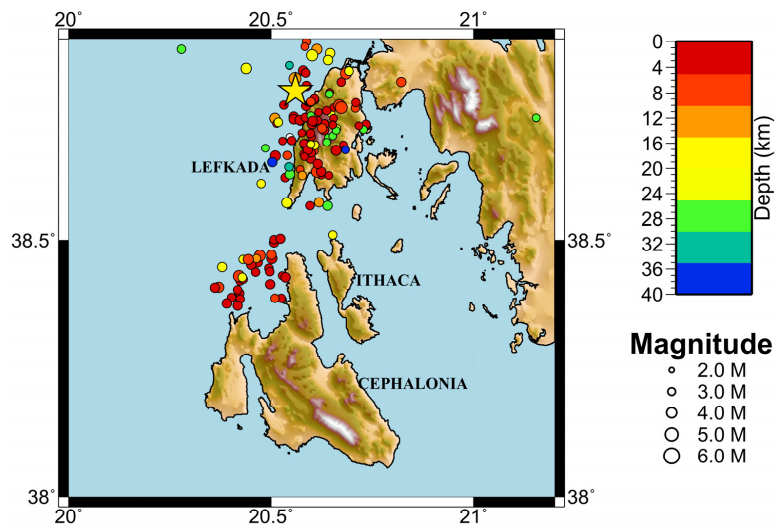


Figure 13. Map showing the Lefkada 2003 aftershock sequence as located by NOAGI. Only the events located with at least 6 phases are shown.

2732

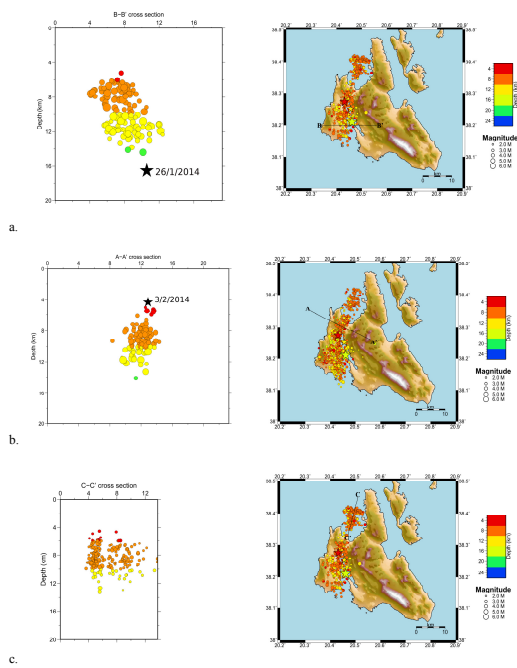


Figure 14. Vertical sections of the aftershock sequence and their location maps (a) The section depicts the hypocenters (with $GAP < 180^\circ$) between 26–30 January 2014 (b) The section depicts the hypocenters (with $GAP < 180^\circ$) between 3–8 February 2014 (c) The section depicts the hypocenters (with $GAP < 180^\circ$) between 26–30 January 2014.